Ab initio based determination of thermodynamic properties of cementite including vibronic, magnetic, and electronic excitations

A. Dick,* F. Körmann, T. Hickel, and J. Neugebauer
Max-Planck-Institut für Eisenforschung GmbH, D-40237, Düsseldorf, Germany
(Received 24 January 2011; revised manuscript received 23 May 2011; published 1 September 2011)

The thermodynamic properties of cementite have been evaluated with a hybrid approach, which describes the vibrational and electronic excitations based on density functional theory calculations, while the magnetic free energy is evaluated using the spin quantum Monte Carlo scheme. Our ansatz allows us to calculate the heat capacity and free energy of cementite with a high accuracy resulting in a free-energy difference of less than 10 meV/atom at 1500 K when compared with experiment. For the formation energy of cementite we observe, however, that the accuracy of density functional theory within the Perdew-Burke-Ernzerhof exchange-correlation functional is not sufficient to provide quantitative agreement with experiment. We show that the main limit in the accuracy of this exchange-correlation functional is the $T = 0$ K potential energy surface.

DOI: 10.1103/PhysRevB.84.125101 PACS number(s): 64.60.Ej, 71.15.Mb, 75.40.Cx, 75.50.Bb

I. INTRODUCTION

The phase diagram of Fe-C plays an essential role in understanding and tailoring thermodynamic properties of carbon-containing steels. Cementite (Fe_3C) is one of the key structures appearing in the Fe-C phase diagram, and is the predominant carbide in carbon steels.[1] Among others, it allows one to control the mechanical properties of steels by combining the hard and brittle cementite phase with the soft and ductile phase of α-Fe (ferrite). Fe_3C has also attracted significant attention in geophysics due to a recent suggestion that it can be contained in the Earth's core.[2–4] An experimental evaluation of the cementite properties is, however, not trivial since at ambient pressure it is a metastable phase up to $\approx$1000 K,[5] and the experimental samples are typically contaminated with ferrite and bulk carbon phases.[6] This leads to a sizable scatter between different experimental studies when considering the thermodynamic properties of cementite, such as the thermal volume expansion, heat capacity, and the heat of formation. Consequently, an unambiguous parametrization of experiment-based thermodynamic databases within, for example, the CALPHAD concept, becomes cumbersome. In this situation supplementing experimental data sets with results of first-principles calculations becomes appealing, since the latter have the main advantage of not using any fitting parameters. In case of cementite, however, the majority of the first-principles studies are focused so far on $T = 0$ K properties only,[7–13] and do not take temperature effects into account, thus providing only limited input to experimental databases.

In a recent paper[14] we have presented a hybrid approach which combines first-principles electronic structure total energy calculations with quantum Monte Carlo simulations in order to assess the thermodynamic properties of cementite. In the present paper we extend that work by providing a detailed description of the obtained results as well as of the underlying methodologies. The results obtained using this approach are compared with a recent thermodynamic assessment of Fe_3C, where particular emphasis has been put on the accurate description of the free energy. We further consider the thermodynamic stability of cementite versus the decomposition into the bulk carbon and iron phases, and discuss the accuracy and errorbars of the free energy for each individual phase.

II. METHODOLOGY

The thermodynamic properties of Fe_3C are calculated assuming that the various excitation mechanisms are adiabatically decoupled. This allows us to decompose the Helmholtz free energy $F(T,V)$ into three contributions:

$$F(V,T) = F^{\mathrm{vib}}(V,T) + F^{\mathrm{el}}(V,T) + F^{\mathrm{mag}}(V,T). \quad (1)$$

Here F^{vib}, F^{el}, and F^{mag} are the free energy contributions due to lattice vibrations and electronic and magnetic excitations, respectively.

To calculate F^{vib} we use the quasiharmonic approximation[15,16] which accounts for the thermal expansion of the crystal $V_0(T)$ based on the explicit description of the phonon properties at different crystal volumes as obtained with the density-functional theory (DFT). In order to calculate the dynamical matrix we have employed the direct force constant method with atomic displacements of ± 0.02 Å from the atomic equilibrium positions and using five volumes homogeneously spanning the volume range between $V_0(T = 0\ \mathrm{K})$ and $1.06 \cdot V_0(T = 0\ \mathrm{K})$. The projector augmented wave method[17] within the generalized gradient approximation in Perdew-Burke-Ernzerhof (PBE) parametrization[18] as implemented in the VASP[19] package was used in the corresponding calculations. Iron and carbon PAW potentials include $3d$ and $4s$, as well as $2s$ and $2p$ states as valence, respectively.

The convergence of the calculated vibrational contribution is ensured by using a supercell consisting of $2\times2\times2$ Fe_3C unit cells (128 atoms), plane-wave energy cutoff $E_{\mathrm{cut}} = 400$ eV, $\approx$13 000 $\boldsymbol{k}$-points per atom resulting from a homogeneous Monkhorst-Pack sampling of the Brillouin zone. A first order Methfessel-Paxton scheme with a thermal smearing parameter of 0.15 eV is used for integration over the $\boldsymbol{k}$-points. A homogeneous mesh of more than 10^6 $\boldsymbol{q}$ points has been used to integrate over the phonon spectrum in the reciprocal space. We note, that in case of cementite explicit systematic convergence tests of F^{vib} with respect to the supercell size are not straightforward: The $1\times1\times1$ cell (16 atoms) is too small to ensure high convergence of the vibrational free energy, while the $3\times3\times3$ supercell (432 atoms) is computationally too expensive. We have, therefore, compared ferromagnetic Fe_3C with ferromagnetic bcc Fe as a reference, for which systematic convergence tests are computationally feasible.

In particular, we have analyzed the force constant versus distance distribution for 128-atom Fe_3C supercell (minimum interatomic distance between an atom and its image $a > 8.9$ Å) with that in bcc-Fe 54-atom supercell ($a \approx 8.5$ Å). We have found, that for both systems the distributions are even quantitatively similar: for distances larger than 3.5 Å the largest force constants do not exceed 0.15 eV/Å^2, while for distances up to 3.5 Å the largest force constants decrease from $\approx$10 eV/Å^2 to $\approx$1.5 eV/Å^2. Based on this comparison we expect the F^{vib} convergence for Fe_3C is similar to that in bcc Fe, where for 54-atom large supercell F^{vib} is converged to better than $\approx$1 meV/atom at $T = 1300$ K.

The phonon calculations for Fe_3C are performed assuming a ferromagnetic ordering of the system at all volumes. The magnetic moments at each volume are calculated self-consistently, that is, without applying constrains within the DFT calculations. This results in an increase of the local magnetic moments of the Fe atoms with increasing volume. This magnetovolume effect is, however, weak: for the volume which corresponds to $T = 1500$ K the increase of the local magnetic moments of Fe when compared to that at $V_0(T = 0\ \mathrm{K})$ is less than 0.1 μ_{B} (compared to the absolute value of the Fe local magnetic moments at V_0 of $\approx$1.9 μ_{B}, see Table I). Thus, in the relevant temperature interval the local magnetic moments in the ordered magnetic state remain essentially unchanged. The phonon calculations are, therefore, decoupled from the electronic temperature-driven excitations, including the excitations of the local magnetic moments. For bcc iron it was recently shown by Shang *et al.*[20] that the influence of magnetic order on the vibronic contribution on the Helmholtz free energy can be accounted for by considering different magnetic structures and a statistical averaging procedure. The extension and application of these concepts[20] beyond simple magnets toward more complex magnetic alloys such as the considered cementite structure, is a topic of ongoing research and is beyond the scope of the present manuscript.

The electronic contribution $F^{\mathrm{el}}(V,T)$ is calculated using finite temperature DFT,[21,22] which explicitly describes the excess energy of the thermally excited electrons at a given T. For this purpose a $\boldsymbol{k}$-point mesh with $\approx$40 000 $\boldsymbol{k}$-points per atom and a Fermi-Dirac statistics was used. Identical to the quasiharmonic calculations, a nonconstrained ferromagnetic collinear state of the system is assumed at all temperatures. Further method details on the *ab initio* calculations of $F^{\mathrm{vib}}(V,T)$ and $F^{\mathrm{el}}(V,T)$ are discussed in Ref. 15.

The magnetic free energy $F^{\mathrm{mag}}(V,T)$ is described by solving the quantum Heisenberg model for the Fe_3C crystal. A promising approach to numerically solve the quantum Heisenberg model is given by the spin quantum Monte Carlo approach (QMC). For many realistic systems such as bcc iron, the long-ranged magnetic exchange interactions result, however, into spin frustration causing the so-called negative sign problem[23] and making the QMC approach inapplicable. Mapping the long-ranged Heisenberg model onto an effective nearest-neighbor Heisenberg model provides a frustration free system that can be readily solved using QMC. The application to the transition metals iron, cobalt, and nickel revealed the high efficiency and excellent performance of this approach.[24] In this work we therefore employ the same methodology to compute the magnetic contribution of cementite. The three ingredients to construct the nearest-neighbor model are the crystal structure, the effective spin quantum number and the effective nearest-neighbor exchange parameter J. Whereas the first ingredients are obtained by first-principles directly, the latter is determined by the experimental critical temperature $T_C^{\mathrm{exp}} = 483$ K.[25] We note that due to the atomic relaxations the averaged nearest-neighbor distance for Fe_{8d} and Fe_{4c} slightly differs (2.61 ± 0.04 Å for Fe_{8d} and 2.57 ± 0.06 Å for Fe_{4c}). Since these differences are one order of magnitude smaller than the second nearest-neighbor distance (approximately 3.7 Å), the same effective J is chosen for all considered first nearest neighbors.

We performed spin QMC calculations using the ALPS code[26] and employing the direct-loop algorithm and local updates within the stochastic series expansion representation. The magnetic contribution of the C atoms is neglected since their local magnetic moments are found to be negligible (less than 0.006 μ_{B}) compared to that of the Fe species. The calculations have been performed using a supercell consisting of $6 \times 6 \times 6$ Fe_3C unit cells (3456 atoms), and 5×10^6 steps for thermalization and statistical averaging. Since the localized spin model only permits multiple of half integer spin quantum numbers ($S_{\mathrm{Fe}} = 0, 1/2, 1, \ldots$), the magnetic free energy for Fe_3C with the equilibrium local magnetic moments of the Fe atoms $M_{\mathrm{Fe}}^{\mathrm{eq}}(T = 0\ \mathrm{K}) \approx 1.9\ \mu_{\mathrm{B}}$ (see Table I) is calculated using linear interpolation between the spin QMC free energies evaluated with the spin quantum number $S_{\mathrm{Fe}} = 1$ as well as $S_{\mathrm{Fe}} = 1/2$. These numbers for the Fe atoms correspond to $M_{\mathrm{Fe}} = 2\ \mu_{\mathrm{B}}$ and $M_{\mathrm{Fe}} = 1\ \mu_{\mathrm{B}}$, respectively, with the Landé factor $g \approx 2$ being used.[27] In the spin QMC calculations the $T = 0$ K value of the $M_{\mathrm{Fe}}^{\mathrm{eq}}$ was used at all temperatures.

The temperature-dependent free energy of formation (formation energy) of Fe_3C from the bulk iron and carbon phases is calculated as

$$\Delta F_f(T) = F_{\mathrm{Fe_3C}}(T) - [3F_{\mathrm{Fe}}(T) + F_{\mathrm{C}}(T)]/4. \qquad (2)$$

Here all free energies F are given per atom. $F_{\mathrm{Fe}}(T)$ is taken from Ref. 24, where it was calculated using the identical approach as employed here for Fe_3C. In Ref. 24, however, the plane-wave cutoff energy $E_{\mathrm{cut}} = 340$ eV was sufficient to ensure convergence of the free-energy $F_{\mathrm{Fe}}(T)$ to less than 1 meV/atom up to $T = 1800$ K. Thus, in case of α-Fe the increase of the cutoff energy from $E_{\mathrm{cut}} = 340$ eV to $E_{\mathrm{cut}} = 400$ eV may change the ground-state energy of the crystal $[F_{\mathrm{Fe}}(0)]$, but does not change the temperature dependence of the free energy $\Delta F_{\mathrm{Fe}}(T) = F_{\mathrm{Fe}}(T) - F_{\mathrm{Fe}}(0)$ within the accuracy margins. In this work we, therefore, calculate the free energy of α-Fe corresponding to $E_{\mathrm{cut}} = 400$ eV as $F_{\mathrm{Fe}}(T) = F'_{\mathrm{Fe}}(T) + \Delta E_{\mathrm{ecut}}$, where $\Delta E_{\mathrm{ecut}} = E_{\mathrm{tot}}^{\mathrm{Fe}}(340\ \mathrm{eV}) - E_{\mathrm{tot}}^{\mathrm{Fe}}(400\ \mathrm{eV})$, and $F'_{\mathrm{Fe}}(T)$ is the α-Fe free energy calculated with $E_{\mathrm{cut}} = 340$ eV.

We note here that apart from the above described spin QMC scheme for calculating the *ab initio* magnetic free energy F^{mag}, an alternative approach to compute this contribution is employing the random phase approximation (RPA) and solving the complete (not effective) Heisenberg Hamiltonian analytically.[28–30] In a previous study on α-Fe it has been found that employing the RPA within Eq. (1) allows us to calculate

the free energy of this material with an accuracy comparable to that within the spin QMC method (less than 20 meV/atom at $T = 1500$ K).[27] In the following we will apply both *ab initio* approaches to describe the magnetic contribution of $F_{\mathrm{Fe}}(T)$ in Eq. (2). The simultaneous application of both approaches has the advantage that the sensitivity of $\Delta F_f(T)$ on the free-energy methodology (for α-Fe) as well as possible error cancellations when using QMC (for α-Fe as well as Fe_3C) can be assessed.

$F_{\mathrm{C}}(T)$ in Eq. (2) is the free energy of a bulk carbon phase. The thermodynamically stable phase of bulk carbon is graphite which is experimentally known to be at $T = 0$ K about 5–20 meV/atom more stable than diamond.[14,31,32] Accordingly, the properties of the carbon ground-state phase are in the literature often described employing GGA-DFT for graphite. However, it is well known that conventional DFT exchange-correlation functionals fail to accurately describe the weak correlation forces of van der Waals type. Therefore, another established approach to calculate the total energy of the graphite phase in $\Delta F_f(T = 0\ \mathrm{K})$ is the use of the diamond structure as a reference, and the subsequent application of an energy shift of ≈5–20 meV/atom in favor of graphite.[14,33] There is no justification, however, that the latter procedure can be used to describe the free energy of graphite at finite temperatures. In order to estimate the importance of van der Waals interactions in the system we calculate $\Delta F_f(T)$ considering not only graphite, but also the diamond reference for carbon.

The diamond and graphite calculations are performed using the identical PAW potential and employing a plane-wave cutoff energy of $E_{\mathrm{cut}} = 400$ eV as for Fe_3C. In the case of diamond the calculations are fully converged with respect to this parameter. In the case of graphite this applies only to the in-plane geometry, while the interlayer spacing is continuously increasing with an increase of the cutoff energy. To be more specific, the in-plane lattice constant changes only from $a_0 = 2.469$ Å to $a_0 = 2.467$ Å when increasing the cutoff energy from $E_{\mathrm{cut}} = 400$ eV to $E_{\mathrm{cut}} = 1500$ eV, that is, by less than 0.1%. In contrast, for the out-of-plane lattice constant the corresponding change is from $c_0/a_0 = 2.871$ to $c_0/a_0 = 3.600$. This indicates that the PBE xc functional predicts extremely weak bonding between the graphene sheets, which is characterized by a rapid step-like change from the high-electron charge density in the vicinity of the graphene sheets to the low-electron charge density in between the sheets. Consequently, an accurate description of such a step-like distribution of the electron charge density along the out-of-plane direction requires extremely high plane-wave cutoff energies, leading to the above mentioned slow convergence of c_0. Fortunately, the spurious increase of c_0 has little effect on the formation energy of Fe_3C (less than 2 meV/atom difference between, e.g., $E_{\mathrm{cut}} = 400$ and 800 eV) in which we are interested in the present study.

The convergence of the ground-state calculations for the bulk carbon phases with respect to the $\boldsymbol{k}$ points is ensured by using more than 13 000 (18 000) homogeneously distributed $\boldsymbol{k}$ points per atom in case of diamond (graphite).

The calculations of the free energy $F_{\mathrm{C}}(T)$ are performed using Eq. (1), with the magnetic contribution being zero. The supercell sizes used in the quasiharmonic phonon calculations are $3 \times 3 \times 3$ (216 atoms) and $6 \times 6 \times 1$ (144 atoms) for diamond and graphite, respectively. The electronic $F_{\mathrm{C}}^{\mathrm{el}}(V,T)$ is calculated using the same settings as for the ground-state calculations. A homogeneous mesh of more than 5×10^5 $\boldsymbol{q}$ points has been used for the integration over the first Brillouin zone.

III. THERMODYNAMIC PROPERTIES

A. Ground-state properties

The ground-state properties of cementite have been intensively studied by first-principles calculations, and, regarding structural and magnetic properties, are known to be rather accurately predicted by DFT with GGA xc functionals. Considering the $T = 0$ K enthalpy of formation ΔF_f [see Eq. (2)], the best agreement with experiment is obtained when using DFT data for graphite without any corrections that could account for missing van der Waals contributions and disregarding the zero-point energy. When ΔF_f is calculated approximating the graphite ground-state energy by shifting that of diamond (see discussion in Sec. II), the agreement with experiment worsens. The obtained agreement when neglecting van der Waals interactions is probably related to error cancellation and is thus coincidental.

The corresponding results of the present study are summarized in Table I, together with selected first-principles and experimental data for comparison. In order to estimate the impact of the frozen-core approximation, which is used to describe the electron-ion interactions in the present work, we compare our calculations with the results of all-electron studies, where the overall accuracy of the calculations is limited only by the specific form of the employed xc functional. The comparison in Table I indicates that our calculations are in perfect agreement with previous PAW studies, and that the assumption of a frozen core has only a marginal influence on the accuracy of the calculated properties of Fe_3C. In fact, the deviations of the results due to use of another gradient-corrected xc functional (PW91 instead of PBE) are larger than that due to the frozen-core approximation. Excluding the experimental work of Duman *et al.*[6,43] where an unusually low equilibrium volume has been reported (see Table I), our calculations predict an equilibrium volume at $T = 0$ K that is about 2% smaller than the experimental volume at this T (see Fig. 1).

B. Thermal volume expansion

The quasiharmonic analysis using the parameters described in Sec. II shows that ferromagnetic Fe_3C is dynamically stable at all considered volumes and temperatures, that is, no phonons with imaginary frequencies in the relevant volume range are found. In Fig. 1 we show the calculated thermal volume expansion of cementite in comparison with available measured data. First, we note some scattering of the measured data, which is comparable with the deviations between our calculations and the measurements. The overall quantitative agreement between the experiment and the calculations is remarkable and is within 2% for the atomic volume at all considered temperatures. We note that the kink observed in the experimental curves at T_C is not reproduced within our

TABLE I. Calculated energetic, structural, and magnetic properties of cementite in comparison with selected experimental and theoretical data. V_0 is the equilibrium volume per unit cell, a_0, b_0, and c_0 are the corresponding lattice constants, B_0 and B_0' are the bulk modulus and its derivative at V_0, and $m_{\mathrm{Fe_{4c}}}$ and $m_{\mathrm{Fe_{8d}}}$ are local magnetic moments of Fe atoms. The formation energy of Fe_3C at $T = 0$ K, ΔF_f, is calculated taking the graphite structure for the carbon reference (superscript "a" indicates that the latter is obtained by introducing an energy shift of 20 meV/atom relative to the diamond structure, superscript "b" indicates that a graphite energy as obtained with DFT is used), or using the diamond structure (indicated with superscript "c"). Superscript "d" indicates the values correspond to $T = 298$ K. Superscript "f" indicates that the values correspond to the heat of formation. Superscript "g" shows estimation of the heat of formation to $T = 0$ K (Refs. 10 and 45). The formation energy of Fe_3C, calculated in the present work including the zero-point energy, is given in brackets.

V_0 (Å^3)	a_0 (Å)	b_0 (Å)	c_0 (Å)	B_0 (GPa)	B_0'	$m_{\mathrm{Fe_{4c}}}$ (μ_B)	$m_{\mathrm{Fe_{8d}}}$ (μ_B)	ΔF_f (meV/atom)	Method	Reference
Theory ($T = 0$ K)										
151.49	5.035	6.716	4.480	213	4.36	1.92	1.84	19.5(−13.7)[a] 45.6(24.3)[b] 14.5(−8.7)[c]	PAW/PBE	present results
153.49[d]	5.053[d]	6.745[d]	4.503[d]	196[d]	5.37[d]					
151.71	5.037	6.720	4.482	–	–	1.97	1.88	20.6[a], 16.4[c]	PAW/PBE	Ref. 33
151.95	5.024	6.754	4.478	234	4	–	–	45[b]	PAW/PBE	Ref. 12
152.2	5.128	6.665	4.462	227	–	2.06	1.96	55.8[b]	FLAPW/PBE	Ref. 8
152.8	5.047	6.743	4.490	–	–	–	–	–	FLAPW/PBE	Ref. 9
153.56	5.068	6.714	4.513	235	–	1.97	1.96	–	FLAPW/PW91	Ref. 11
Experiment ($T = 298$ K)										
154.2–155.4	5.08–5.09	6.73–6.75	4.51–4.53	174 ± 6	4.8 ± 0.8	–	–	37–60[f]	XRD, Calor.	Refs. 2,25,34–42
151.0	5.04	6.73	4.48	174 ± 8	–	1.8 (averaged)		47.5[g]	EELS, XMCD	Refs. 6,43,44

theoretical model. To include it the coupling between magnetic and phononic degrees should also be taken into account. However, such an extension goes beyond the scope of the present paper and is not considered here since the effect is small.

C. Magnetization

The theoretical temperature dependence of the magnetization in comparison with the corresponding experimental data is shown in Fig. 2. The theoretical magnetization is evaluated according to the methodology presented in Sec. II. A full quantitative comparison between theory and experiment is hampered by the fact that the reported experiments were done on multiphase samples containing phase mixture of cementite, ferrite, and carbon. Nevertheless, as shown in Fig. 2, qualitatively the magnetization in Fe_3C is reproduced well and is similar to that for the unary bulk ferromagnetic phases of Fe, Cr, and Ni.[24]

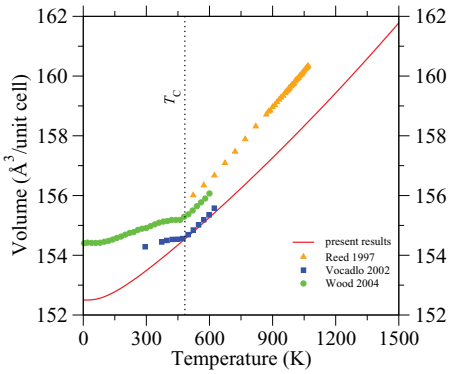

FIG. 1. (Color online) Calculated thermal volume expansion of Fe_3C in comparison with experimental data.

D. Heat capacity

In Fig. 3 the calculated constant pressure heat capacity C_P, available experimental C_P data sets, and results of the phenomenological experiment-based thermodynamic assessments are presented.[46–48] The theoretical heat capacity is split into vibronic, electronic, and magnetic contributions.

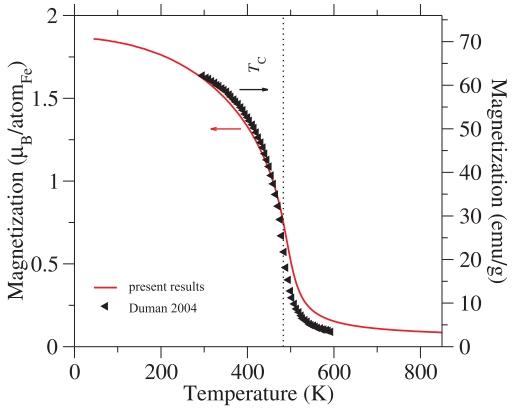

FIG. 2. (Color online) Dependence of the simulated Fe_3C net magnetization on temperature as compared to the experimental data from Ref. 6. The experimental data are acquired at a magnetic field of 5 kOe for a mixture of Fe_3C nanoparticles of size 40 ± 10 nm with the residual carbon and α-Fe with the amount of about 2% by weight for the latter. The calculated magnetization of Fe_3C at $T = 0$ K corresponds to ≈177 emu/g.

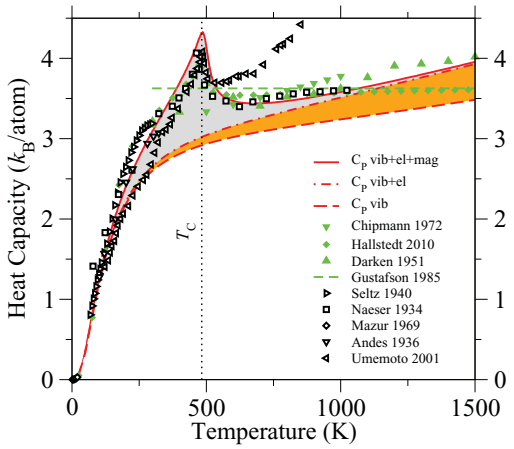

FIG. 3. (Color online) Calculated heat capacity (C_P at $p = 0$) of cementite as a function of temperature T in comparison with available experimental data (open symbols) and thermodynamic assessments (filled symbols). The calculated electronic and magnetic contributions to the heat capacity are shown in shaded orange and gray correspondingly.

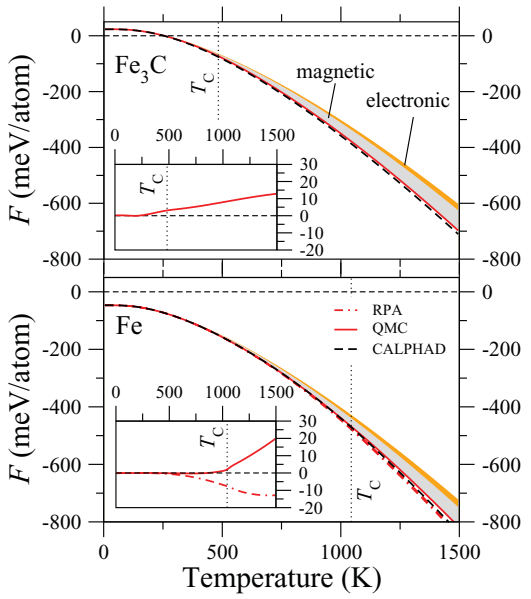

FIG. 4. (Color online) Comparison of the calculated free energies for α-Fe and Fe_3C at zero pressure with the thermodynamic assessment from Ref. 14, referred to as CALPHAD. The first-principles and the CALPHAD curves are aligned at $T = 200$ K. The calculated electronic and magnetic contributions to the free energy are shown in shaded orange and gray correspondingly. The first-principles magnetic free energy is calculated either employing QMC or RPA approach. In the latter case the free energy is extracted from Ref. 27 as described in Sec. II. Inset: The CALPHAD data are taken as reference at each temperature.

Similar to nonmagnetic metals and to α-Fe,[15,27] we find that the dominating contribution originates from the vibronic excitations. We also observe a significant contribution of electronic excitations, which is due to the high density of electronic states close to the Fermi level in Fe_3C.[8] The magnetic part of the heat capacity is largest at the Curie temperature due to the break down of the long-range magnetic order, and smoothly vanishes to zero for temperatures below 200 and above 1000 K.

Comparing our results with the available measurements of the heat capacity at constant pressure (Fig. 3) below the Curie temperature we find that our predicted theoretical curve falls within the scatter of the various measurements. (The large discrepancy of the measured heat capacity in Ref. 25 is unclear and likely related to the quality of the samples and/or their preparation procedure.) Above T_C our curve is located practically on top of the measurements of Naeser,[49] and reproduces the presence of a local minimum at $T \approx 600$ K and the increase at higher temperatures. These results are also consistent with the thermodynamic assessments by Chipmann[5] and Darken *et al.*[50] There is a strong deviation between the above described behavior and the recent measurements by Umemoto and co-workers where C_P steeply increases with the temperature above T_C.[25] In the latest assessment of C_P by Hallstedt *et al.*[14] the heat capacity above 600 K is constant and below it coincides with the experiments of Seltz *et al.*[51] The assessment agrees within the 0.3 k_B/atom with first-principles results up to $T = 1500$ K. In the following we use the Hallstedt *et al.*[14] assessment as reference when comparing other quantities such as the free energy. We note that due to the large scatter in the experimental data underlying the Hallstedt *et al.* assessment, benchmarks are subject to an uncertainty that will hopefully be reduced in the future by progress in materials synthesis and experimental setups.

E. Free energy

In Fig. 4(a) we compare our calculated free energy $F_{Fe_3C}(T)$ with the thermodynamic assessment by Hallstedt *et al.*, which we refer later in the text as CALPHAD assessment or experimental free energy. Since CALPHAD assessments are only extrapolated to low temperatures and are therefore less reliable at temperatures below 200 K,[15] we align the calculated $F_{Fe_3C}(T)$ with the corresponding experimental curve at $T = 200$ K. This allows us to quantitatively analyze the accuracy of the description of the T dependence (excitation of the system) within our theory and to disregard for the moment the accuracy at $T = 0$ K (ground-state properties).

The obtained agreement of the theoretical and the experimental free energies is below 15 meV/atom up to $T = 1500$ K. Similar to α-Fe [see Fig. 4(b)], deviations between the first-principles and the experimental data sets start around T_C [see inset in Fig. 4(a)]. Overall the theoretical free energy of bulk iron and bulk cementite are described with similar accuracy. Deviations from the corresponding experimental results increase with T, with the largest deviation of less than 20 meV/atom at $T = 1500$ K.

It is noteworthy that qualitative use of the QMC for the magnetic part provides for both systems underestimated free energy F. When using an analytic RPA solution for the magnetic part which is shown in Fig. 4(b) for sake of completeness for α-Fe, the first-principles free energy is slightly overestimated compared to experiment. It could be of interest to figure out, therefore, whether the same behavior

holds for other elements and systems such as, e.g., Fe_3C, which could indicate that these two solutions of the Heisenberg model (RPA and effective QMC) bound the true solution.

IV. PHASE STABILITY

The construction of an accurate *ab initio* Fe-C phase diagram requires one to calculate the thermodynamic stability of different phases with respect to each other. For the case of Fe_3C the relevant bulk phases are α-Fe and graphite. Recalling that conventional semilocal DFT exchange-correlation functionals (like GGA-PBE used here) fail to correctly describe van der Waals interactions, we consider next to the graphite phase (where van der Waals interactions between the graphene layers are large) also diamond as reference for carbon. While the latter phase does not appear in the Fe-C phase diagram it can be easily computed in a CALPHAD approach and allows us to thus estimate the importance of van der Waals interactions in the system (see discussion in Sec. II). The calculated free energies of all these phases are shown in Figs. 4 and 5.

Using Eq. (2) and the data shown in Figs. 4 and 5, we analyze the phase stability for Fe_3C. A positive formation energy indicates that Fe_3C is thermodynamically unstable against a decomposition into bulk Fe and C phases. The resulting calculated heat of formation $\Delta F_f(T)$ obtained when using either the graphite or the diamond as a reference phase for C in comparison with the corresponding CALPHAD data is shown in Fig. 6.

First, we focus on the zero-temperature enthalpy of formation. Vibrational zero-point energies (ZPE) significantly influence the formation free energy of Fe_3C. Indeed, while the ZPE contributions for cementite and α-Fe are nearly identical

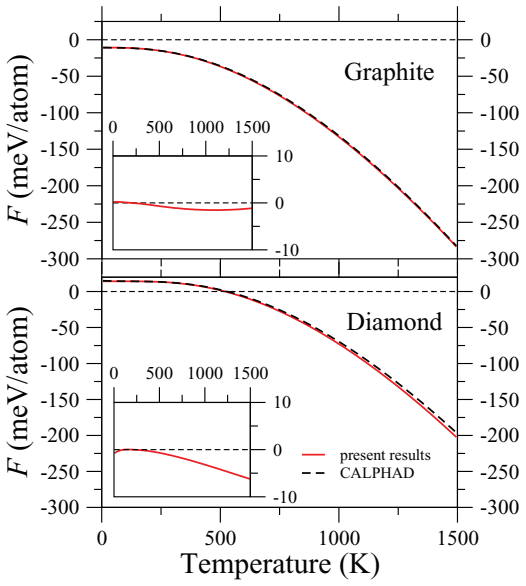

FIG. 5. (Color online) Comparison of the calculated free energies for diamond and graphite at zero pressure with the thermodynamic assessments from Ref. 14 (graphite) and the THERMOCALC program with the SGTE unary database[52] (diamond), referred to as CALPHAD. The first-principles and the CALPHAD curves are aligned at $T = 200$ K. Inset: The CALPHAD data are taken as reference at each temperature.

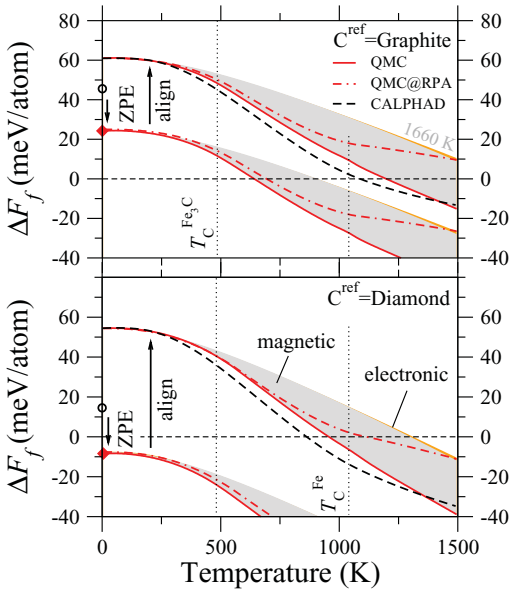

FIG. 6. (Color online) Calculated free energy of formation of cementite from the pure compounds (bcc Fe and graphite) at zero pressure as a function of temperature and including zero-point vibrations (upper figure). Results obtained when assuming the diamond phase (where van der Waals interactions are absent and which is used only as a benchmark) are shown in the lower figure. The open black circles show the $T = 0$ K data without zero-point vibrations. The black dashed curve, referred to as CALPHAD, gives the thermodynamic assessment as given in Ref. 14 (for α-Fe, Fe_3C, graphite) and the THERMOCALC program with the SGTE unary database[52] (diamond), based on experimental data. For an easier comparison of the temperature dependence the present theoretical curves aligned to the CALPHAD value at $T = 200$ K are also shown. The calculated electronic and magnetic contributions to the free energy are shown in shaded orange and gray correspondingly. The first-principles magnetic free energy for Fe_3C is calculated either employing QMC approach, while for α-Fe either QMC or RPA approach is used. In the latter case the free energy is extracted from Ref. 27 as described in Sec. II. The temperature at which $\Delta F_f(T) = 0$ when the magnetic free energy of α-Fe and Fe_3C is neglected ($T \approx 1600$ K) is shown in gray (upper figure).

(52 and 41 meV/atom, respectively) and cancel each other, the ZPE of the carbon phase (178 or 170 meV/atom when considering diamond or graphite, respectively) is significantly larger. As a result, the total decrease of ΔF_f due to zero-point vibrations is about 20-25 meV/atom (see Table I). Taking into account that the predicted energy of formation at $T = 0$ K is even without including ZPE lower than the corresponding CALPHAD data, this leads to an underestimation of the calculated ΔF_f by ≈33 and 63 meV/atom when taking graphite and diamond, respectively. Moreover, if we consider the theoretical diamond phase as a reference in our calculations and introduce the free energy of graphite by using the commonly accepted energy shift of 20 meV/atom in favor of graphite, the first-principles formation energy of cementite versus graphite is underestimated by about 50 meV/atom (Table I). In this case our calculations predict Fe_3C to be thermodynamically stable at all temperatures. Only if taking

the first-principles results for graphite as reference we obtain Fe_3C to be unstable at temperatures below ≈650 K (see Fig. 6).

To identify the reasons for the large absolute shift between our calculations and the experimental data we first compare our results with all-electron first-principles calculations for the formation energy of Fe_3C as well as for the cohesive (atomization) energy of bulk C, α-Fe, and Fe_3C. This data is collected in Tables I and II. First, we note that the frozen-core approximation, which underlies the present calculations, results in about 10 meV/atom underestimation of the zero-temperature heat of formation of Fe_3C (see Table I). The all-electron and PAW ΔF_f using the graphite phase as a reference essentially coincides with the CALPHAD assessment if zero-point energies are not included. Assuming that the ZPE contribution calculated with the PAW and the all-electron methodology are not significantly different, we conclude that it is the current form of the xc functional which results in an underestimation of the zero-temperature ΔF_f by about 25 meV/atom when using graphite as a reference for carbon.

According to Eq. (2) the deviation in the calculated ΔF_f originates from a poor description of one or several of the reference structures (bulk C, Fe, and/or Fe_3C). To identify the structure that is likely responsible for the major part of the deviations we consider the cohesive properties of bulk C, Fe, and Fe_3C (Table II). The strength of the chemical bond is overestimated by the PBE xc functional for all phases. The deviations are most significant for α-Fe and Fe_3C with about 1.1 and 0.8 eV/atom too high cohesive energies, respectively, while for both carbon phases the deviation from the corresponding experimental value is less than 0.4 eV/atom. This indicates that the PBE xc functional is not accurate enough in predicting the cohesive properties of all the considered structures, but in particular those containing Fe as a chemical species.

Inspecting Fig. 6 we find that the agreement between our *ab initio* calculations and the CALPHAD data assuming graphite as reference is better than assuming diamond as reference for the CALPHAD and the *ab initio* calculations. This is a rather remarkable result and contradicts conventional wisdom according to which diamond should be more accurately described than graphite where van der Waals interactions occur that are absent in the DFT calculations employed here. We therefore conclude that the error introduced by the xc functional has an opposite sign than the van der Waals interaction so that in case of graphite a partial error compensation occurs. This insight may be used to better understand limitations of present xc functionals and eventually to construct improved ones.

In order to separate the errors in describing ground-state and finite temperature effects, we align the theoretical ΔF_f with the CALPHAD curves at $T = 200$ K. The aligned curves are also shown in Fig. 6. We separate again magnetic and electronic contributions in order to identify the shift of the stable-unstable transition temperature when the corresponding contribution is excluded. In Fig. 6 we also compare the results with calculations using a mixed description of the magnetic part, that is, F^{mag} for α-Fe is described within the RPA and for Fe_3C within the QMC scheme.

First, we note, that the when focusing on the temperature dependence of $\Delta F_f(T)$, using both the graphite and the benchmark diamond structures results in a similar accuracy. This indicates that in our case missing van der Waals interactions in case of the graphite do not significantly influence the accuracy of the calculated $\Delta F_f(T)$. Second, we note the essential differences which appear when mixing RPA and QMC results as compared to data obtained when consistently using QMC for both magnetic systems. In case of graphite the use of the mixed scheme leads to an increase of the transition T by about 300 K, which clearly indicates that in case of Fe_3C an accurate description of the magnetic excitations above T_C might be as important as that below the critical magnetic temperature. Out of these two approaches taking the QMC method for Fe_3C and for α-Fe gives a consistently better quantitative agreement with the CALPHAD curve. Indeed, focusing on the corresponding ΔF_f and using an alignment at $T = 200$ K the predicted temperature at which the cementite becomes thermodynamically stable is only ≈100 K above the corresponding CALPHAD value. Since the fitted CALPHAD heat capacity is slightly different from the corresponding theoretical dependence, we cannot expect a perfect agreement between the two data sets, and minor quantitative differences are, therefore, natural. It is also noteworthy that the free energy of electronic excitations is almost vanishing for ΔF_f (e.g.,

TABLE II. Calculated cohesive energies (neglecting and including ZPE) for diamond, graphite, α-Fe, and Fe_3C in comparison with various experimental and theoretical data.

System	E_{coh} (eV/atom)	$E_{\mathrm{coh}}^{\mathrm{ZPE}}$ (eV/atom)	Method	Reference
Diamond	7.82	7.64	PAW-PBE	present results
	7.86	–	FLAPW-PBE	Ref. 32
	–	7.37	Expt.	Refs. 24, 33 from Ref. 32
Graphite	7.94	7.77	PAW-PBE	present results
	7.99	–	FLAPW-PBE	Ref. 32
	–	7.38	Expt.	Refs. 24, 33 from Ref. 32
α-Fe	5.27	5.23	PAW-PBE	present results
	5.11	–	FLAPW-PW91	Ref. 53
	–	4.28	Expt.	Refs. 95, 96 from Ref. 53
Fe_3C	5.89	5.84	PAW-PBE	present results
	–	5.05	Expt. estimate	Ref. 54

ΔF_f^{el} is less than 2 meV/atom at $T = 1500$ K), while the magnetic contributions are essential (e.g., $\Delta F_f^{\mathrm{mag}}$ is more than 20 meV/atom at $T = 1500$ K) and their neglect leads to an increase of the transition T by ≈300–450 K.

V. SUMMARY

Performing a carefully converged hybrid approach of DFT and spin QMC we find that the thermodynamic properties of Fe_3C can be computed with a high degree of accuracy. The quantitative deviations from the available experimental measurements are found to be smaller than 2% and 0.3 k_B/atom for temperatures up to 1500 K for the atomic volume and the heat capacity, respectively. It is interesting to note that the deviation of the present theoretical data from experiment are often smaller than the experimental scatter, indicating that our present available functionals are excellently suited to describe the T dependence of thermodynamic data.

A comparison of our results for the T dependence of the free energy of Fe_3C with our recent experimental assessment shows that these energies differ by less than 10 meV/atom up to $T = 1500$ K, with the maximum deviation at the highest temperature. For lower temperatures the agreement between the experimental and the theoretical data set gradually improves. This behavior is consistent with the previously reported application of this methodology to α-Fe, where a maximum deviation of 25 meV/atom at $T = 1500$ K was reported.[27]

To evaluate the thermodynamic stability of Fe_3C against decomposition into bulk Fe and C phases we have calculated the free energy of formation of cementite. We find that the thermal excitations are accurately described within the present theory, predicting, for example, the transition temperature only ≈100 K above the corresponding CALPHAD value. Such an agreement is remarkable when taking into account the uncertainty, which persists in the thermodynamical assessment. In order to consistently improve the accuracy of the T-dependent properties within the framework of the current theoretical model higher order effects like phonon-phonon and phonon-magnon interactions, longitudinal fluctuations of the local magnetic moments, and possible temperature-activated effects such as the creation of various point defects (e.g., vacancies, interstitial C atoms, etc.), and possible off-stoichiometry of the compound have to be included.

Our calculations indicate that the zero-temperature formation energy in cementite as calculated with GGA-DFT deviates from the CALPHAD assessments in the order of 50 meV per atom. This leads to a large discrepancy between the calculated and the CALPHAD-based stability of Fe_3C. Since the T dependence of the theoretical formation energy is described with a high degree of accuracy, this indicates that the main limitation of the existing exchange-correlation functionals is in the $T = 0$ K potential energy surface, consistent with previous findings for nonmagnetic metals.[15]

ACKNOWLEDGMENTS

The authors thank Blazej Grabowski and Bengt Hallstedt for fruitful discussions. Financial support of the collaborative research center SFB 761 "Stahl - *ab initio*" of the Deutsche Forschungsgemeinschaft and the Interdisciplinary Center for Materials Simulation (ICAMS), which is supported by ThyssenKrupp AG, Bayer MaterialScience AG, Salzgitter Mannesmann Forschung GmbH, Robert Bosch GmbH, Benteler Stahl/Rohr GmbH, Bayer Technology Services GmbH, and the state of North-Rhine Westphalia as well as the European Commission in the framework of the European Regional Development Fund (ERDF), is gratefully acknowledged.

*a.dick@mpie.de

[1] C. M. Fang, M. H. F. Sluiter, M. A. van Huis, C. K. Ande, and H. W. Zandbergen, Phys. Rev. Lett. **105**, 055503 (2010).
[2] H. P. Scott, Q. Williams, and E. Knittle, Geophys. Res. Lett. **28**, 1875 (2001).
[3] N. L. Chabot, A. J. Campbell, W. F. McDonough, D. S. Draper, C. B. Agee, M. Humayun, H. C. Watson, E. Cottrell, and S. A. Saslow, Geochim. Cosmochim. Acta **72**, 4146 (2008).
[4] O. Lord, M. Walter, R. Dasgupta, D. Walker, and S. Clark, Earth Planet. Sci. Lett. **284**, 157 (2009).
[5] J. Chipman, Metall. Trans. **3**, 55 (1972).
[6] E. Duman, M. Acet, T. Hülser, E. F. Wassermann, B. Rellinghaus, J. P. Itié, and P. Munsch, J. Appl. Phys. **96**, 5668 (2004).
[7] C. Ande and M. Sluiter, Acta Mater. **58**, 6276 (2010).
[8] J. H. Jang, I. G. Kim, and H. Bhadeshia, Comput. Mater. Sci. **44**, 1319 (2009).
[9] A. K. Arzhnikov, L. V. Dobysheva, and C. Demangeat, J. Phys. Condens. Matter **19**, 196214 (2007).
[10] G. Miyamoto, J. Oh, K. Hono, T. Furuhara, and T. Maki, Acta Mater. **55**, 5027 (2007).
[11] H. I. Faraoun, Y. D. Zhang, C. Esling, and H. Aourag, J. Appl. Phys. **99**, 093508 (2006).
[12] K. O. E. Henriksson, N. Sandberg, and J. Wallenius, Appl. Phys. Lett. **93**, 191912 (2008).
[13] S. Khmelevskyi, A. V. Ruban, and P. Mohn, J. Phys. Condens. Matter. **17**, 7345 (2005).
[14] B. Hallstedt, D. Djurovic, J. von Appen, R. Dronskowski, A. Dick, F. Körmann, T. Hickel, and J. Neugebauer, Calphad **34**, 129 (2010).
[15] B. Grabowski, T. Hickel, and J. Neugebauer, Phys. Rev. B **76**, 024309 (2007).
[16] L. N. Kantorovich, Phys. Rev. B **51**, 3520 (1995).
[17] P. E. Blöchl, Phys. Rev. B **50**, 17953 (1994).
[18] J. P. Perdew, K. Burke, and M. Ernzerhof, Phys. Rev. Lett. **77**, 3865 (1996).
[19] G. Kresse and J. Furthmüller, Phys. Rev. B **54**, 11169 (1996).
[20] S.-L. Shang, Y. Wang, and Z.-K. Liu, Phys. Rev. B **82**, 014425 (2010).
[21] N. D. Mermin, Phys. Rev. **137**, A1441 (1965).
[22] G. M. J., J. Phys. Condens. Matter **1**, 689 (1989).

[23]F. Körmann, A. Dick, T. Hickel, and J. Neugebauer, Phys. Rev. B **81**, 134425 (2010).
[24]F. Körmann, A. Dick, T. Hickel, and J. Neugebauer, Phys. Rev. B **83**, 165114 (2011).
[25]M. Umemoto, Z. Liu, K. Masuyama, and K. Tsuchiya, Scr. Mater. **45**, 391 (2001).
[26]A. Albuquerquea, F. Aletb, P. Corboza, P. Dayala, A. Feiguind, S. Fuchse, L. Gampera, E. Gulla, S. Gürtlerf, A. Honeckere *et al.*, J. Magn. Magn. Mater. **310**, 1187 (2007).
[27]F. Körmann, A. Dick, B. Grabowski, B. Hallstedt, T. Hickel, and J. Neugebauer, Phys. Rev. B **78**, 033102 (2008).
[28]M. Pajda, J. Kudrnovsky, I. Turek, V. Drchal, and P. Bruno, Phys. Rev. B **64**, 174402 (2001).
[29]G. Y. Gao, K. L. Yao, E. Şaşoğlu, L. M. Sandratskii, Z. L. Liu, and J. L. Jiang, Phys. Rev. B **75**, 174442 (2007).
[30]J. Rusz, L. Bergqvist, J. Kudrnovský, and I. Turek, Phys. Rev. B **73**, 214412 (2006).
[31]J. Harl and G. Kresse, Phys. Rev. Lett. **103**, 056401 (2009).
[32]J. V. Badding and T. J. Scheidemantel, Solid State Commun. **122**, 473 (2002).
[33]C. M. Fang, M. A. van Huis, and H. W. Zandbergen, Phys. Rev. B **80**, 224108 (2009).
[34]S. Meschel and O. Kleppa, J. Alloys Compd. **257**, 227 (1997).
[35]W. Roth, Z. Angew. Chem. **42**, 981 (1929).
[36]L. Vočadlo, J. Brodholt, D. P. Dobson, K. S. Knight, W. G. Marshall, G. D. Price, and I. G. Wood, Earth Planet. Sci. Lett. **203**, 567 (2002).
[37]R. C. Reed and J. H. Root, Scr. Mater. **38**, 95 (1997).
[38]K. H. Jack, Proc. R. Soc. Lond. Math. Phys. Sci. **195**, 56 (1948).
[39]H. Okamoto, J. Phase Equilib. **13**, 543 (1992).
[40]I. G. Wood, L. Vocadlo, K. S. Knight, D. P. Dobson, W. G. Marshall, G. D. Price, and J. Brodholt, J. Appl. Crystallogr. **37**, 82 (2004).
[41]J. Li, H. K. Mao, Y. Fei, E. Gregoryanz, M. Eremets, and C. S. Zha, Phys. Chem. Miner. **29**, 166 (2002).
[42]B. J. Wood, Earth Planet. Sci. Lett. **117**, 593 (1993).
[43]E. Duman, M. Acet, E. F. Wassermann, J. P. Itié, F. Baudelet, O. Mathon, and S. Pascarelli, Phys. Rev. Lett. **94**, 075502 (2005).
[44]I. N. Shabanova and V. A. Trapeznikov, JETP Lett. **18**, 339 (1973).
[45]D. R. Lide (ed.), *CRC Handbook of Chemistry and Physics* (CRC, Boca Raton, FL, 2009).
[46]R. V. Andes, Iowa State College J. Sci. **11**, 26 (1936).
[47]J. Mazur and W. Zacharko, Acta Phys. Polon. **35**, 91 (1969).
[48]P. Gustafson, Scand. J. Metall. **14**, 259 (1985).
[49]G. Naeser, Mitt. Kais.-Wilh. Inst. Eisenforschg. **16**, 207 (1934).
[50]L. S. Darken and R. W. Gurry, J. Met. **3**, 1015 (1951).
[51]H. Seltz, H. J. McDonald, and C. Wells, Trans. AIME **140**, 263 (1940).
[52]A. F. Guillermet and P. Gustafson, High Temp. High Press. **16**, 591 (1985).
[53]C. Elsässer, J. Zhu, S. G. Louie, M. Fähnle, and C. T. Chan, J. Phys. Condens. Matter **10**, 5081 (1998).
[54]J. Häglund, A. Fernández Guillermet, G. Grimvall, and M. Körling, Phys. Rev. B **48**, 11685 (1993).